LCLS-TN-01-9
7 November 2001

Imaging, weakly-perturbing diagnostics of an x-ray beam at the LCLS facility (physics issues)

A. Wootton, D. Ryutov

Lawrence Livermore National Laboratory, Livermore, CA 94551

Abstract

Several approaches to the imaging of the x-ray beam cross-section in the LCLS facility have been proposed: deflecting a small part of the beam by a thin mirror; partial scattering from a thin, high-density gas jet, partial scattering from a thin solid foil. The general feature of all these diagnostics is that the imaging does not introduce significant perturbations to the beam. A set of design equations and constraints is provided.

I. INTRODUCTION

The LCLS x-ray beam consists of several components [1], of which the most important are: 1) the first harmonic of the coherent radiation; 2) the third harmonic of the coherent radiation; 3) the spontaneous radiation. At the nominal energy of the electron beam, 14.35 GeV, the photons of the first harmonic will have an energy of 8 keV and a 1.5 Å wavelength; the photons of the third harmonic have 24 keV and 0.5 Å, respectively. Spontaneous radiation has a broad spectrum extending from tens of electron-volts to hundreds of kilo-electron-volts. The system can operate with an electron beam energy lower than the nominal energy; the X-ray spectrum then is shifted to lower energies. The lowest energy of the fundamental that we will consider is 800 eV. An x-ray beam will be generated in short pulses, ~250 fs long, with a repetition frequency of 120 Hz.

In this paper we present a preliminary analysis of the diagnostics that would allow one to obtain a time-integrated image of the beam cross-section in every pulse, and would also provide an absolute calibration of the number of photons in the beam. One of the most important requirements of such diagnostics is that they do not significantly perturb the x-ray beam, and the beam, after its image had been obtained, remains suitable for the further use in the experiments. We shall concentrate on the optics of the imaging system and will not discuss at any depth equally important issues of the detection system proper.

There are a variety of experiments planned at the LCLS facility ranging from high-energy-density physics to biophysics [2]. A specific experiment requires normally only one component of the beam. Some of the experiments will be carried out close to the beam exit from the undulator, whereas the others will be housed in experimental halls hundreds of meters downstream. The x-ray beam experiences a natural diffraction-limited divergence and its diameter varies significantly along the beam path (e.g., from ~ 120 μm to ~ 600 μm for an 8 keV component). The need to diagnose a broad range of energies

and beam cross-sections is a difficult task. E.g., the diagnostics designed for the measurements of the fundamental at 8 keV may not be suitable for the measurements of the fundamental at a reduced energy, say, 800 eV. Likewise, the diagnostics working at relatively low fluences in the far experimental halls may not work near the undulator.

In the present preliminary study we do not pretend to cover all the possible combinations of the beam energy and beam diameter. We would rather present discussion of several particular cases, which, however, may serve as guidance for a more general assessment.

The separation of the beam components is also a difficult problem, especially if one wants to get rid of the higher-energy x-rays and work only with the lower energy ones (e.g., getting rid of the 24 keV component and working with the 8 keV component only). The separation problem is closely coupled to the beam diagnostics. A general strategy in the separation of the components could be a deflection of the lower-energy part by a grazing-incidence mirror or a multilayer, which would not affect the higher-energy component. As the reflected beam may suffer perturbations of the wave front, this reflecting element should be situated as close to the experimental object as possible; the diagnostics would then be situated between this element and the object. The spontaneous radiation has normally a much larger angular divergence than the fundamental and the third harmonic; it can, therefore, be cut off by a collimator.

We start our discussion with the fundamental at 8 keV (Sec. II), first in the nearest (to the undulator) experimental hall and then in the furthest hall. This section is the longest and the most important section of the report, as it contains general equations that can be used for the other photon energies. After that, we briefly consider diagnostics of the third harmonic at 24 keV (Sec. III), of the spontaneous radiation (Sec. IV), and of the fundamental at 800 eV, i.e., for the reduced energy of the electron beam (Sec.V). In Sec. VI we discuss the ways of separating various beam components. Finally, Sec. VII contains a summary of our results.

II. DIAGNOSTICS OF AN 8 KEV BEAM

A. Thin reflecting foil of a low-Z material

1. General layout

The idea of this diagnostics is to place a thin foil of a low-Z material in the way of the beam, in grazing incidence geometry (Fig. 1). The tilt angle θ (Fig. 1) must be small, so as to provide a relatively high reflectivity R, which scales as $1/\theta^4$ at small θ (until θ approaches the critical angle θ_{crit} of the perfect external reflection).

The foil must be thin, so that the beam absorption in the foil be small. This constraint on the foil thickness h can be presented as

$$\mu h / \sin\theta << 1 \qquad (1)$$

where μ (cm^{-1}) is a linear absorption coefficient ($dI/dz = -\mu I$). The reflected light, which forms an almost parallel beam, will then be collected by a detection system D situated at some distance L from the beam axis. One will therefore obtain a time-integrated

distribution of the beam intensity over its cross-section. As mentioned in the Introduction, we do not consider specific implementation of the detection system here.

The total number of 8 keV photons in a single LCLS pulse is expected to be [1]

$$N = 2 \cdot 10^{12}, \tag{2}$$

with the energy per pulse

$$E = 2.6 \text{ mJ}. \tag{3}$$

The beam radius in the first experimental hall will be approximately

$$r = 60 \ \mu\text{m}. \tag{4}$$

In this first rough assessment we will neglect effects of x-ray polarization and assume that the initial beam is un-polarized. In discussion of a possible role of photons experiencing incoherent scattering in the foil, we assume that the scattering is isotropic. A more complete picture will be considered in the further analyses.

We shall make all the numerical estimates for a beryllium foil, although our general expressions are applicable to other materials. At room temperature, the number density of atoms, n, is (in the beryllium)

$$n = 1.24 \cdot 10^{23} \text{ cm}^{-3}. \tag{5}$$

The absorption coefficient μ is [3]:

$$\mu = 1.9 \text{ cm}^{-1}. \tag{6}$$

It is determined mostly by the photoabsorption (~85%) and inelastic scattering (~15%); some (minor) contribution comes from elastic scattering. The cross-section for the inelastic scattering is

$$\sigma_{scatt} = 1.74 \cdot 10^{-24} \text{ cm}^2 \tag{7}$$

As the binding energy of electrons in Be atoms is significantly less than the energy of the incident x rays, the energy of the scattered x rays will be close to their initial energy of 8 keV.

2. The foil tilt

If the tilt angle is of the order of unity, the reflectivity R is very small (for $\theta = 45^0$ it is of the order of 10^{-11}), and the number of photons N^* available for detection,

$$N^* = 2NR, \tag{8}$$

is only 40 and insufficient to reach any reasonable spatial resolution. Note that x rays are reflected from both front and rear surfaces of the foil, whence the coefficient "2" in the equation for N^*.

This consideration pushes us in the direction of small θ (grazing incidence). Assuming that 10^5 photons are sufficient for attaining good spatial resolution, one finds that the reflectivity must be $2.5 \cdot 10^{-7}$. According to [3], in the case of a perfectly flat surface, this corresponds to $\theta = 80$ mrad (4.5^0). The critical angle is 3 mrad, i.e., much smaller. The reflectivity at such relatively large θ is sensitive to the surface roughness and decreases dramatically if the surface roughness is more than a few angstroms. This

favors even shallower angles, where surface roughness is much less important. As a compromise between roughness problem and increased complexity associated with using too shallow angles, we suggest using

$$\theta = 40 \text{ mrad } (\theta = 2.3^0). \tag{9}$$

At such a tilt the absorption of the LCLS x-ray beam in a mirror is still insignificant. Indeed, for a foil thickness

$$h = 4 \text{ μm}, \tag{10}$$

the fraction of the absorbed energy $\Delta E/E$ is:

$$\frac{\Delta E}{E} = \frac{\mu h}{\sin\theta} \approx 0.02 \tag{11}$$

We have used here Eqs. (6) and (9).

3. Constraints on the foil thickness.

We see that absorption in the foil does not impose too severe constraints on the foil thickness. If this constraint was the only one, one could even increase the foil thickness to 20 or so micrometers, thereby simplifying the handling of the foil. Unfortunately, there exist two more constraints, which push us towards the use of thinner foils. The first and the most obvious one is the loss of spatial resolution caused by the shift of the images produced by reflections from the front and the rear sides of the foil (Fig. 2). This shift ξ can be found from the relation:

$$\xi = 2h\cos\theta \approx 2h\,. \tag{12}$$

If one wants to reliably discern the features whose size constitutes a fraction ε of the beam radius r, then ξ must satisfy an inequality $\xi < \varepsilon r$, or equivalently, h must satisfy an inequality

$$h < \frac{\varepsilon r}{2} \tag{13}$$

For quite a modest value of ε, $\varepsilon = 0.2$, the foil must be thinner than 6 μm.

The second constraint stems from the necessity to reduce the relative amount of the light incoherently (and, as we assume, isotropically) scattered by beryllium atoms. The relative contribution of this factor is proportional to the foil thickness. (The contribution of scattered photons decreases for shallower incidence angles, because the reflectivity grows much faster than $1/\theta$). The total number of scattered photons can be evaluated as:

$$N_{scatt} = \frac{hn\sigma_{scatt}}{\sin\theta} N \tag{14}$$

For the set of parameters as in Eqs. (5), (7), (9) and (10), and the foil thickness of 4 μm, one has

$$\frac{N_{scatt}}{N} \approx 2.2 \cdot 10^{-3} \tag{15}$$

This is four orders of magnitude greater than the relative number of reflected photons. However, scattered quanta fill in the 4π solid angle, and only a small fraction of them end up on the surface of the detection system. Even if one does not use any material limiters, the number of scattered photons hitting the same spot as an image of the reflected beam is small compared to N_{scatt} , and can be evaluated as

$$\pi r^2 \frac{N_{scatt}}{4\pi L^2} \tag{16}$$

To have this number smaller (by some large factor C) than the number of reflected photons N^*, one has to satisfy the following condition (see Eqs. (8), (14), and (16)):

$$\frac{Chn\sigma_{scatt} r^2}{4\sin\theta L^2} < R \tag{17}$$

Taking L= 10 cm, C = 20, and the other parameters as before, one finds that the l.h.s. is less than the r.h.s. by two orders of magnitude. In other words, in this specific situation Eq. (17) does not impose an additional constraint on the thickness of the foil. However, if one decides to use larger θ and smaller L, this constraint may become very restrictive. In such a case, the use of a limiter between the foil and the detector may help.

4. The role of surface contamination

There is the probability that the surface of the foil will be coated by a thin film of oxides formed during exposure to the air. Other impurities may be collected because of imperfect vacuum. These heavier impurities may generate K_α lines in the range of hundreds of electron-volts and higher. They would produce an incoherent radiation into the 4π solid angle; part of this radiation will be collected by the detection system in the same way as the scattered radiation. Here, again, moving the detection system further from the foil will reduce the relative contribution of this component. As the energy of characteristic radiation for the most common impurities (like oxygen, nitrogen and carbon) lies below 1 keV, one can also use an absorbing filter (say, a few micrometer thick beryllium foil in front of the detection system) to completely eliminate this part of radiation.

Surface contamination, as well as gradual increase of the surface roughness (the latter caused by non-equilibrium processes during each pulse and, possibly, by periodic temperature variations) may change the foil reflectivity. If these processes occur non-uniformly over the foil surface, this may cause the appearance of non-uniformities of the beam image. The unknown variation of reflectivity may also create problems with absolute calibration of the system.

5. Alignment issues

If the foil is displaced by some distance η along the normal to the foil, the reflected beam gets shifted by the distance $2\eta\cos\theta$ (Cf. Eq. (12)). (The displacement in the tangential direction, obviously, does not cause any changes in the position of the reflected beam). As a result, the whole imprint of the reflected beam gets simply displaced along

the surface D in Fig. 1. If this displacement is smaller than the aperture of the detection system, this does not cause too serious problems.

A deviation $\delta\theta$ of the tilt from the desired tilt θ also causes the displacement of the beam image. This displacement is equal to $2L\delta\theta$. Imposing a constraint that this displacement must be less than the beam diameter, one finds that $\delta\theta$ must satisfy a rather severe constraint:

$$\delta\theta < \frac{r}{L} \tag{18}$$

For L = 10 cm this yields $\delta\theta$ < 0.6 mrad.

An even more strict constraint must be imposed on the possible non-planarity of the foil surfaces. If the surfaces of the film are somewhat wavy, then the images created by reflection from the two surfaces are distorted, generally speaking, differently from each other. In order to be able to resolve features of the scale εr, one has then to impose a constraint on the angle $\delta\theta_1$ (Fig. 3) characterizing the deviation of the surface from the plane:

$$\delta\theta_1 < \frac{\varepsilon r}{2L} \tag{19}$$

For the modest value of ε, ε = 0.2, and for L = 10 cm, one obtains that $\delta\theta_1$ < 60 μrad. In particular, two sides of the foil must be parallel with the accuracy better than 60 μrad. This planarity constraint must be satisfied on the scale $2r/\theta \sim 3$ mm, corresponding to the large axis of the beam imprint on the reflecting foil.

6. Interference effects.

The waviness of the foil surface may cause the appearance of an interference pattern on the plane D. If, for example, the foil is slightly bent in the middle, so that the two parts form a small angle $\delta\theta < \varepsilon r/2L$ with respect to each other, an interference pattern with the distance between the maxima $\delta y = \lambda/4\delta\theta$ will be formed (λ = 1.5 Å is the wavelength of x rays). However, for all realistic (i.e., not *too* small) values of $\delta\theta$ this δy is very small compared to the features of the order of εr we are interested in.

7. Heating of the foil.

The temperature increase after the passage of a single pulse is

$$\Delta T = \frac{E\mu}{\pi r^2 c_p} \tag{20}$$

where c_p is specific heat. For beryllium, it is 3.3 J/cm^{3}K. Taking the other parameters from Eqs. (3), (4), and (6), one finds that $\Delta T \approx$ 13 K. This is a modest temperature increase, which would probably not cause any problems. We leave evaluation of the resulting thermal stresses and deformations for the further work.

Of some concern may be an average increase of the temperature produced by a continuous sequence of the pulses, at the frequency f = 120 Hz. The average heat flux has to be accommodated by a frame that would hold the foil (Fig. 4). The strongest average

temperature increase will occur near the center of the beam. Assuming that the frame is held at a constant ambient temperature, one finds that

$$\langle \Delta T \rangle = \Delta T \frac{r(2b-r)f}{2\chi} \tag{21}$$

where χ is thermal diffusivity of the foil (for beryllium, $\chi =$ 0.52 cm^2/s) and b is the width of the frame (Fig. 4). Taking b = 300 μm and the other parameters as before, one finds that $<\Delta T>$ = 0.45 K. This seems to be acceptable, as thermal deformation of the foil will be quite small, satisfying even a very strict constraint (19).

B. Gaseous jet

1. General outline

Another possible imaging diagnostic is based on the use of a gaseous jet intersecting the beam as shown in Fig. 5. Photons scattered incoherently by the atoms of the jet could then be imaged to the detector by a pinhole (*P*, in Fig. 5). All the numerical examples in this section will be made for a neon jet, although general equations are applicable for other materials.

The use of a strongly collimated supersonic jet (instead of a gas-filled volume, which could also serve as a scatterer of the beam photons off the beam-line) helps in two respects: first, it greatly simplifies the system for the differential pumping, compared to the one that would be required in the case of a gas-filled volume (Cf. [4]); second, a small thickness of the jet, under some circumstances (see Sec. II.B.3), helps to improve the spatial resolution of the system.

The nozzle from which the jet emerges is situated behind the plane of the Figure. Its orifice is a strongly elongated rectangle. The smaller dimension determines the thickness of the jet, h, whereas the larger dimension determines its width, w. The tilt of the jet allows increasing the column density of the gas on the beam path (as $1/\sin\theta$).

The cross-sections for the photoabsorption and scattering of 8 keV photons in neon are [3]:

$$\sigma_{abs} = 7.5\cdot 10^{-22} \text{ cm}^2;\ \sigma_{scatt} = 3.5\cdot 10^{-24} \text{ cm}^2 \tag{22}$$

2. Total number of photons collected by the detection system

As we have already stated in Sec. I.1, in this preliminary analysis we assume that the scattered photons are distributed isotropically. Then, the number of photons projected by the pinhole *P* to the plane *D* can be evaluated as

$$N^*_{scatt} = \frac{Nn\sigma_{scatt}h}{\sin\theta}\cdot\frac{\pi a^2}{4\pi L_1^2}, \tag{23}$$

where n is the number density of atoms in the gaseous jet, a is the pinhole radius, and L_1 is defined on Fig.5. The first factor in Eq. (22) is the total number of scattered photons, whereas the second factor is a fraction of these photons passing through the pinhole aperture; N is the total number of beam photons per pulse, Eq. (2).

For numerical estimates, we assume that n is ten times higher than the number density at normal conditions, i.e.,

$$n = 2.7 \cdot 10^{20} \text{ cm}^{-3}, \tag{24}$$

and that the thickness of the jet is

$$h = 0.5 \text{ mm}. \tag{25}$$

Later, in Sec.II.B.4 we shall discuss the feasibility of generating such jets. With regard to the tilt angle, θ, we assume that it is 0.1 rad:

$$\theta = 0.1. \tag{26}$$

Imposing a constraint that N^*_{scatt} exceeds 10^5, one then finds from Eq. (23) that the ratio a/L_1 must satisfy condition

$$a/L_1 > 0.02 \tag{27}$$

As requirements of a high spatial resolution push us in the direction of smaller a, this inequality can be replaced by an equality, i.e.,

$$L_1 \approx 50a \tag{28}$$

Note that the absorption of the LCLS beam in the neon jet with the aforementioned parameters becomes of some significance, $\Delta E/E \sim 0.1$ (Cf. Eq.(11)).

3. Spatial resolution

We will not discuss here the spatial resolution of the detection system itself (e.g., limitations stemming from the finite number of pixels). We will only discuss the quality of an image produced by the pinhole in the plane D (Fig. 5), which then will be "viewed" by the detector proper.

We assume that the distance L_2 from the pinhole to the plane D is larger than L_1, so that the beam imprint on the jet will be projected with some magnification. In this case, in order to have the features of the size εr be projected without a strong smearing, one has to impose a constraint

$$a < \varepsilon r \tag{29}$$

Assuming that $\varepsilon = 0.2$, and using Eqs. (4) and (28), one finds that the allowable values of both a and L_1 are quite small,

$$a \sim 12 \text{ μm} \tag{30}$$

$$L_1 \sim 600 \text{ μm} \tag{31}$$

The collimator should be made of a relatively high-Z material, in which the attenuation length of the photons would be less than 12 μm, e.g., gold.

As the estimate (31) shows, the collimator has to be situated very close to the intersection point of the beam and the jet. It could then become exposed to a broader (spontaneous radiation) halo of the beam. This would generate stray signals in the detection system. Additional shield cutting off the spontaneous radiation could solve this problem.

The distance L_2 (see Fig. 5 for notation) determines the magnification of the system. L_2 can be made significantly greater than L_1, say, 10 times greater. This would yield an image with the diameter of 1.2 mm.

In principle, by using line of sight close to the direction of the beam, one could produce an image of a cross-section of the beam by a plane normal to its axis. To reach this mode of imaging, one has to use the observation angle θ_1 satisfying the condition:

$$\theta_1 < \frac{r}{(h/\sin\theta)} \tag{32}$$

However, for the parameters as in Eqs. (4), (25), (26) this condition yields an unrealistically small value of θ_1, θ_1<0.012.

The aforementioned difficulties with very small dimensions and small angles stem from a relatively small number of photons scattered from the jet. The real number of photons may, in fact, be somewhat higher: in addition to the scattering, some number of kilo-electron-volt photons will be produced in collisions between photoelectrons and atoms. This contribution may be significant and would allow one to increase L_1 beyond the level determined by Eqs. (23) and (27). The quantitative result is not available at the moment. If this contribution is significant, it must also be taken into account in the absolute calibration of the system. If, on the other hand, one is not interested in these lower-energy photons, one can easily filter them out by placing a thin absorber in front of the pinhole.

A significant simplification of the system can be reached if one agrees to reduce requirement to the total number of photons available for detection, say, $N^* \sim 10^4$ instead of $N^* \sim 10^5$ (this, of course, would increase requirements to the performance of the detection system proper). One would then be able to switch to the geometry shown in Fig. 6, with the jet perpendicular to the beam. As θ is now $\pi/2$, one can satisfy condition (32) at a reasonable value of θ_1 and reach the situation where a 2D imaging would become feasible.

4. Gas flow

We suggest using a supersonic nozzle with a small divergence of the jet, of the type discussed in Ref. 5 (see also a recent publication [6]. The only difference is that we are now going to produce a jet of a rectangular cross-section. We assume that the thickness of the jet is as in Eq. (25) whereas the width w of the jet is 2 mm,

$$w = 2 \text{ mm} \tag{33}$$

At high densities we are interested in the mean free path is much less than the size of the slot, so that the hydrodynamic description of the flow is valid. This yields the following expression for the velocity of the jet outside the nozzle

$$\mathrm{v} = \sqrt{\frac{2\gamma}{\gamma - 1}}\sqrt{\frac{kT}{Am_p}} \tag{34}$$

where γ is the adiabat index, T is the temperature in the plenum from which the gas flows, A is atomic weight, and m_p is the proton mass. For monatomic gases (γ = 5/3) at a room temperature

$$\mathrm{v}(cm/s) \approx \frac{3\cdot 10^5}{\sqrt{A}} \tag{35}$$

Therefore, amount Q of gas exhausted through the nozzle is

$$Q = Am_p hwn\mathrm{v} = 1.3\sqrt{\mathrm{A}}\ \ \mathrm{g/s} \tag{36}$$

In the numerical estimate we used Eqs. (24), (25), (33), and (35).

As the jet is supersonic and has a small divergence, it can be trapped in the differential pumping system of the type discussed in [4], with only a minimum amount of gas coming back to the main volume of the accelerator. The gas collected by the differential pumping system can be recovered with a high efficiency. Making a conservative estimate that 99.5% of the gas is recovered, we find that amount of gas lost during 1 hour of an uninterrupted operation of the gas-jet diagnostics will lead to a loss of $24A^{1/2}$ g of the working gas.

If this amount is too large in terms of the operational cost, one could resort to such measures as using pulsed valves, with the time-segment when the valve is open ~ 200 μs, synchronized with the LCLS pulses. As a prototype, the valve described in Ref. [7] can be used. For a 120 Hz rep-rate, this would reduce the loss of gas by a factor of 25 (but complexity would be added).

5. Another geometry employing a gas jet

If one is prepared to sacrifice 2D imaging in favor of having higher signals or smaller losses of the working gas, one could use a different geometry to obtain a 1D image of the beam. This geometry is shown in Fig. 7. The collimator P has a narrow slot parallel to the beam direction, so that the image of the beam looks like a long rectangle, which is essentially a projection of the beam onto the plane parallel to the propagation direction. Compared to a pinhole of a radius a = 12 μm, the slot of a width $2a$ = 24 μm and a length of 2 mm has a much larger surface area thereby dramatically increasing the number of photons available for detection.

C. Low-Z foil as a scatterer of x-rays

Instead of using the gas jet, one could use a foil as a scatterer, especially in the geometry of Fig.6. For the beryllium foil perpendicular to the beam, even the thickness of

$$h\ = 100\ \mu\mathrm{m} \tag{37}$$

is small in terms of the absorption of the initial beam (see Eq. (11)). The total number of scattered photons is large; according to Eqs. (2), (5), (7), (14), and (37) it is

$$N_{scatt} = 4.3\cdot 10^9 \tag{38}$$

This allows one somewhat increase the distances L_1 and L_2 and make the system somewhat more manageable. Also, because the scatterer is now much thinner than the gaseous jet, one can resolve fine structures by satisfying condition

$$\theta_1 < \frac{\varepsilon r}{h}. \tag{39}$$

For r as in (4), h as in (37), and $\varepsilon = 0.2$, one finds that the r.h.s. is equal to 0.12 (i.e., $\approx 7^0$). This allows one to much more easily accommodate the detection system (without placing it too close to the beam).

D. Diagnostics for the far hall

1. Thin mirror

In principle, the analysis presented in the sections A-C can be applied also to the situation of a much larger beam radius,

$$r \sim 250\ \mu\text{m}, \tag{40}$$

typical for the far hall. However, the dimensions of the diagnostic system become significantly different. In addition, relative importance of various constraints changes quite significantly. So, we discuss here these changes.

First of all, the constraint (13) on the film thickness becomes less restrictive. According to Eq. (13), with the beam radius as in Eq. (40), and $\varepsilon = 0.2$, the foil thickness could be increased to about 25 μm. However, for this thickness, the fraction of radiation absorbed becomes more than 10% (see Eq. (11)). It is technically more challenging to make a perfect plane-parallel foil 4 μm thick and with the width of ~ 1-2 mm. So, we suggest keeping the foil thickness at the level of 10 μm (maintaining it 4-μm thick may be too difficult from the technical standpoint, given that the size of the foil has now to be ~ 1-2 mm). So, we assume that now

$$h = 10\ \mu\text{m}. \tag{41}$$

With these new dimensions, the constraint (13) is now satisfied by a larger margin than in the case of a small beam diameter. On the other hand, the relative number of the Compton-scattered photons increases by a factor 2.5. Still, the margin by which Eq. (17) (a constraint on the scattered flux on the surface D, Fig. 1) is satisfied, remains in the range of ~ 30.

The constraint (19) on the co-planarity of the film surfaces becomes somewhat less restrictive, 0.25 mrad, instead of 40 μrad. Foil heating at the end of each pulse becomes by a factor of 25 weaker than for a narrow beam; an average temperature increase remains the same, provided the supporting frame size increases proportionally to the beam radius.

2. Gas jet

For the same value of the parameter ε (that determines the resolution of the system), one can increase the pinhole radius from 10 μm to 1 mm, and, accordingly, increase the distance L_1 from 600 μm to 2.5 mm. The condition (32) can be now satisfied more easily.

For the same tilt of the jet as given by equation (26), the width of the jet has to be increased, to accommodate an X-ray beam of a larger diameter (0.5 mm instead of 0.12 mm). The minimum width that satisfies this condition is w=5 mm. According to Eq. (35), this causes an increase of the gas flow Q, and, thereby, the load on the differential pumping system. Developing a differential pumping system capable of pumping and recovering ~ 15 g/s of Neon, would require some effort.

3. Solid scatterer of the beam photons.

This technique will work in the same way as described in Sec. II.C. The increase of the X-ray beam radius from 50 to 250 μm results in a significant softening of the condition (38): θ_1 can now be a large angle, ~ 45^0. This makes the system much simpler engineering-wise.

E. Summary for 8 keV photons

We have provided a set of equations required for the engineering design of three detection systems based on: 1) specular reflection of the beam from a thin low-Z foil; 2) beam scattering off a dense supersonic gaseous jet; 3) beam scattering off a low-Z foil.

The advantage of the first system is that it provides a large space for the detection system, at a distance of a few centimeters from the beam. A disadvantage is that the requirements on the foil quality are very severe. Also, although the temperature rise within every pulse, as well as an average temperature increase, is modest, the thermal fatigue after, say, 1 hour of operation (~ 400,000 pulses) may bring up a need for frequent replacement of the foil. Surface roughness must stay below a few angstroms both for small- and large-diameter beams.

The advantage of gaseous jets is that they can operate in a continuous mode without any need for replacing any elements. They can be turned on and off without any need for mechanical realignment of the system (unlike the case of a reflecting foil where one would have to carry out a very fine alignment after replacing the foil). A disadvantage is that one needs to use a small pinhole to reach a good 2D resolution. This forces one to place a collimator with the pinhole very close to the beam and the jet. The extremely small size of the system in the case of a 120-μm diameter beam is a serious problem. In the version where a 1D imaging is used, these constraints become somewhat less restrictive. For a 600 μm diameter beam, the system becomes larger and easier to handle. A problem may arise, however, because of a larger gas throughput needed in this case.

An advantage of the solid scatterer is that it provides a larger number of scattered photons than the gaseous jet of a realistic density and thereby somewhat loosens constraints on the miniaturization of the pinhole section of the detection system. This approach should work well both for a small-diameter and the large-diameter beam. A disadvantage is that relatively frequent replacement of the foil may be needed.

III. DETECTING 24 keV PHOTONS

The 24 keV radiation can be detected by the use of either the gas jet or the scattering foil. The analysis presented in Secs. II.B, II.C can be readily applied to this case. The situation is now much more favorable because the ratio of the absorption cross-section to the scattering cross-section decreases by several orders of magnitude compared to the 8 keV case. Indeed one has for neon [3]:

$$\sigma_{abs} = 2.4 \cdot 10^{-23} \text{ cm}^2, \quad \sigma_{scatt} = 5 \cdot 10^{-24} \text{ cm}^2, \tag{42}$$

Cf. Eq. (21). One can therefore increase the thickness of the gaseous jet and thereby increase the number of scattered photons without causing too strong absorption. Instead of increasing the thickness, one could also use a gas with higher Z, or a higher-pressure gas with lower Z. The same is true for the scattering foil: one can either increase its thickness, or use a foil of a higher-Z material, say, Ti. One has for titanium [3]:

$$\sigma_{abs} = 7.1 \cdot 10^{-22} \text{ cm}^2, \quad \sigma_{scatt} = 10^{-23} \text{ cm}^2. \tag{43}$$

For a 50 μm thick titanium foil the ratio of the number of scattered photons relative to the number of incident photons is $2.8 \cdot 10^{-4}$ (i.e., 3 times greater than for the scattering of 8 keV photons in the beryllium foil of the same thickness); on the other hand, the absorption is less than 20%.

IV. DETECTING 800-EV PHOTONS.

The absorption coefficient for 800 eV photons is orders of magnitude higher than for 8 keV photons. In beryllium, the absorption length is ~ 4 μm [3]. This means that even for a foil oriented normally to the beam only a small amount of the initial beam would pass through the foil. Therefore, the technique based on a partial reflection of the beam (Sec. II.A) will not work. One could try to use an inverse technique: specularly reflecting the major part of the beam in the direction of the experimental target and using for diagnostic purposes a small fraction of the beam that was transmitted through the foil. However, to have a high reflectivity, one would have to use very shallow incidence angles, in the range of 1.5 degrees and, in this case, only an extremely small number of photons would be transmitted through a 4-mm thick beryllium foil.

Scattering from gas does not work, either, because the scattering cross-section does not differ very much from that for 8 keV photons, whereas the absorption cross-section is much larger. The latter means that the gas density must be reduced, but then there will be not enough scattered photons. The same problem would prevent one from using the scattering in a Be foil.

A possible solution could be the use of a multilayer that has a high reflectivity at a large incidence angle (say, 45^0). Then, if the total thickness of the multilayer and substrate is below 10-20 μm, a sufficient amount of radiation would come straight through the multilayer and would be used for the beam imaging, whereas the reflected radiation would be used in the experiments (Fig. 8). A problem with this approach may be damage to the multilayer, especially in the near experimental halls.

V. DETECTING SPONTANEOUS RADIATION

A difficulty with detecting spontaneous radiation is that it has a broad energy spectrum that ranges from tens electron-volts to hundreds kilo-electron-volts (for the nominal energy of the electron beam). Placing essentially any material in front of the beam would cause absorption of the lower energy part of the spectrum. The higher-energy part of the spectrum, starting from a few kilo-electron-volts can be detected by the scattering off the neon jet of the type described in Sec. II.B. An attractive feature of this approach is that the scattering cross-section depends only weakly on the x-ray energy: in the range between 4 keV and 100 keV it varies by only a factor of 3. The energies below 4 keV will be cut off by the jet of any reasonable thickness. In other words, the imaging system will generate an image that covers a very broad energy range of the x-ray beam. As the imprint of the spontaneous radiation has a large radius, in the range of 1 mm, the dimensions of the detection system will be not too small (Cf. Sec. II.D.2).

VI. SEPARATION OF THE BEAM COMPONENTS

As we have already mentioned in the introduction, it is conceivable that, for a specific experiment, only one component of the beam will be needed. In case of 24 keV photons, one can easily eliminate the lower-energy component by placing foils that would completely absorb the 8 eV photons but be transparent enough for the 24 keV photons. The spontaneous radiation component can be cut off by using a collimator with a hole just sufficient to accommodate the 24 keV component; this would reduce the energy content of the spontaneous radiation by 3-4 orders of magnitude. So, it is relatively easy to obtain an almost pure 24 keV beam.

It is more difficult to obtain a pure 8 keV beam. The spontaneous radiation can be eliminated as before, but the 24 keV component cannot be filtered out by the absorbers. One can, perhaps, use either a multilayer, or a grazing-incidence mirror to deflect the 8 keV component, whereas the high-energy component would get through. A concern is that the mirrors can be damaged, especially if used in the near hall. Another concern is that the mirror or multilayer will introduce distortions to the wave-front (in particular, because of their imperfect planarity).

The same technique can be used for the low-energy mode of LCLS, where the fundamental will correspond to 800 eV.

VII. DISCUSSION

We have shown that the imaging diagnostic of the LCLS beam is possible in a broad range of energies for both the fundamental and the third harmonic, both in the near and far experimental halls. For the 8 keV range of energies one can use a variety of techniques, including reflection of a small part of the beam in a thin foil, beam scattering in gaseous jet, and beam scattering in a solid foil. The main problem for the first technique is the extremely high quality of the film required for reaching a reasonable resolution. Also of concern is possible damage to the foil. The main problem for the second technique is the extreme compactness of the system required for obtaining a reasonable number of counts. The third system is most robust and does not need foils of

an exceptional quality (as the first system does). Damage to the foil may make it necessary to replace the foil regularly.

The 24 keV component can be diagnosed by the scattering in both the solid foil and the gaseous jet. Elimination of the lower-energy component could be achieved by the use of an absorption filter.

In the low-energy mode of operation, the fundamental harmonic at 800 eV has to be separated from the third harmonic by a multilayer mirror, and then deflected again, in the direction of the experiment. The small fraction of the beam that would penetrate through this second mirror would then be used for producing the beam image.

We have found it difficult to suggest one single diagnostic that would be applicable for all three beam components, and cover regimes of both low and high electron energies. The optimum diagnostic will depend on the parameters of the x-ray beam. As a general conclusion, one can state that, although the imaging of the x-ray beam by a weakly-perturbing diagnostic is not simple, it is certainly possible. At every x-ray pulse (which will follow at a frequency of 120 Hz), one can obtain an image of the beam that hits the experimental target.

Acknowledgment.

This work was performed under the auspices of the U.S. Department of Energy by University of California Lawrence Livermore National Laboratory under contract W-7405-Eng-48.

References

1. The LCLS Design Study Group. *Linear Coherent Light Source (LCLS) Design Study Report* , Report SLAC-R-521, Stanford University (1998)

2. LCLS - The first experiments. Report of the Scientific Advisory Committee for the Linac Coherent Light Source, September 2000 (2000)

3. B. L. Henke, E. M. Gulliksion , J. C. Davis. *Atomic Data and Nuclear Data Tables*, **54**, 181 (1993)

4. D. Ryutov, A. Toor. "X-ray attenuation cell." UCRL-ID-138125, LCLS Technical Note 00-10, May 2000 (2000)

5. D. Ryutov. "SSPX gas puff," February 2000, unpublished.

6. S. Semushin, V. Malka. "High density gas jet nozzle design for laser plasma production." Review of Scientific Instruments, **72**, 2961, (2001)

7. H. McLean. PhD thesis.

Figures

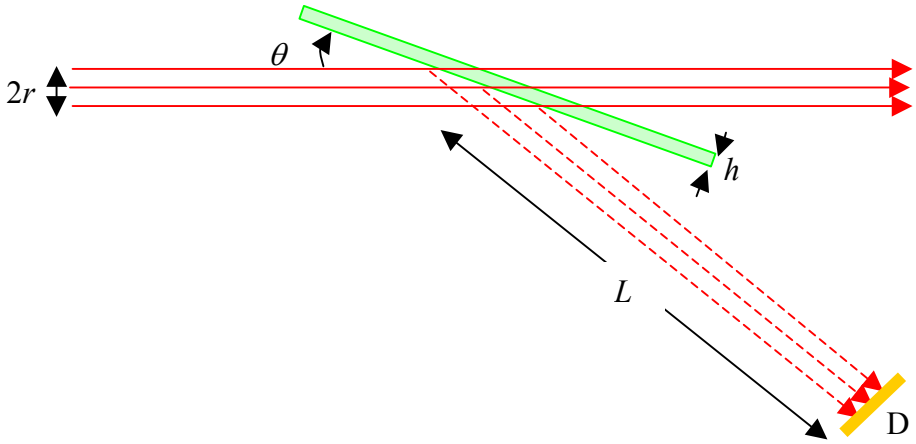

Fig. 1. Imaging of the beam by its specular reflection from a thin foil (shown in green). The reflected beam is shown in dashed lines.

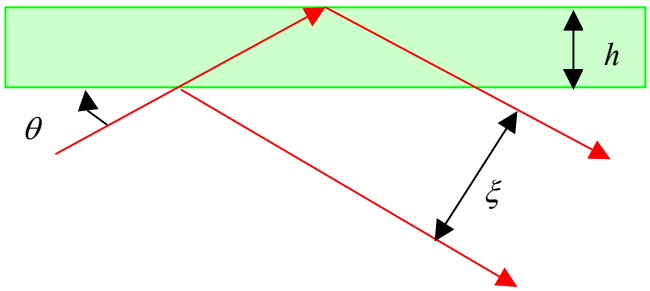

Fig. 2. The geometry needed for the evaluation of the scale of the features blurred by superposition of reflections from two sides of the foil.

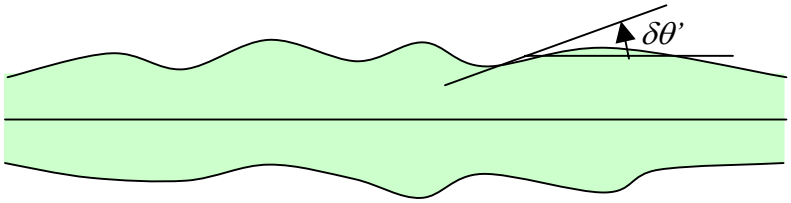

Fig. 3. A non-uniform foil; $\delta\theta'$ is a characteristic tilt of the surface non-uniformities with respect to the ideal planar surface.

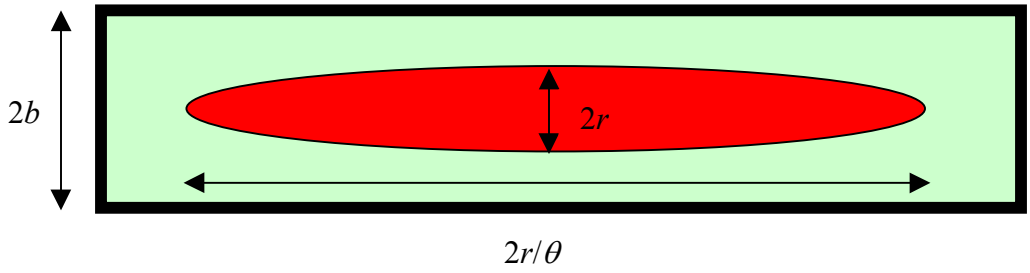

Fig. 4. The beam imprint (red) on the foil (green). Shown in black is a massive supporting frame maintained at a constant temperature.

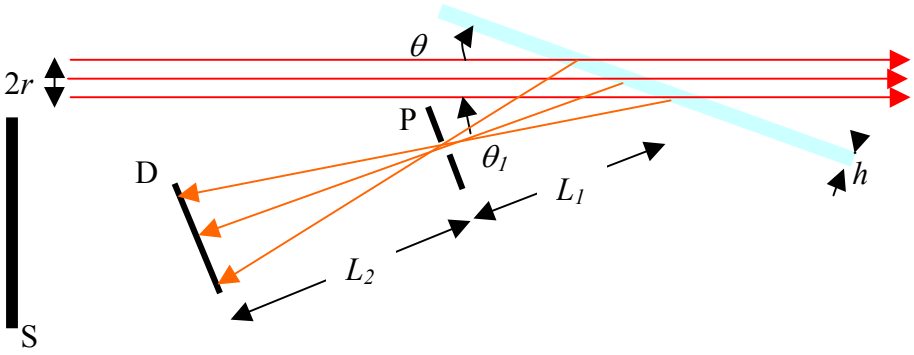

Fig. 5. The cross-section of the gaseous jet is shown in blue; the nozzle is situated behind the figure, and the jet is propagating towards the viewer. Scattered light (orange lines) is projected through a pinhole to the plane D. S is the shield protecting the detection system from a low-energy halo.

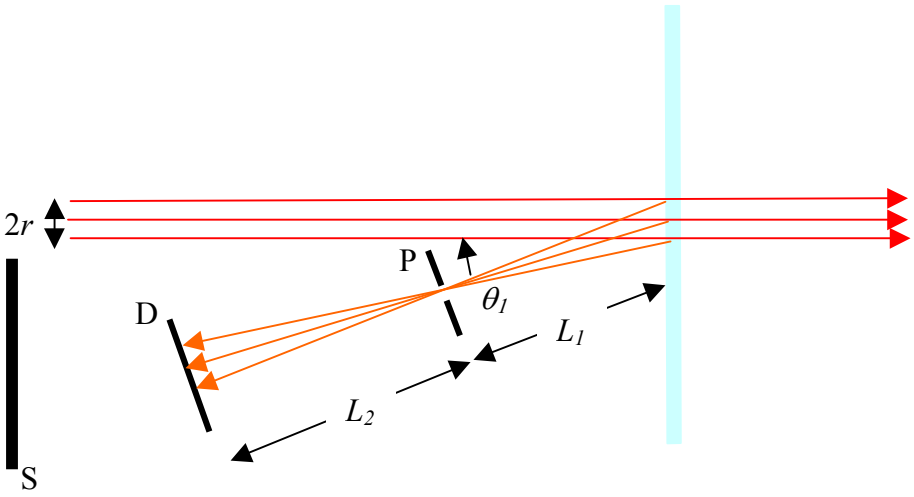

Fig. 6. An alternate geometry, where the jet is normal to the beam. This allows one to obtain 2D images of the beam imprint.

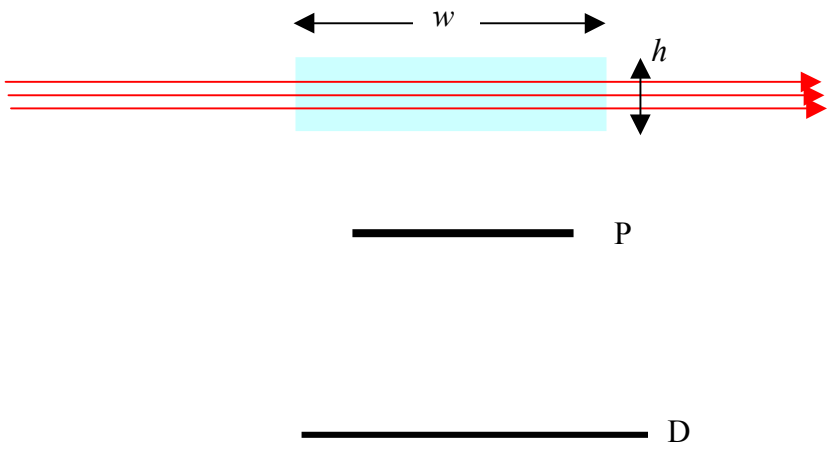

Fig. 7. The projection of the beam through a long narrow slot in the diaphragm P. The slot is along the beam direction and therefore invisible.

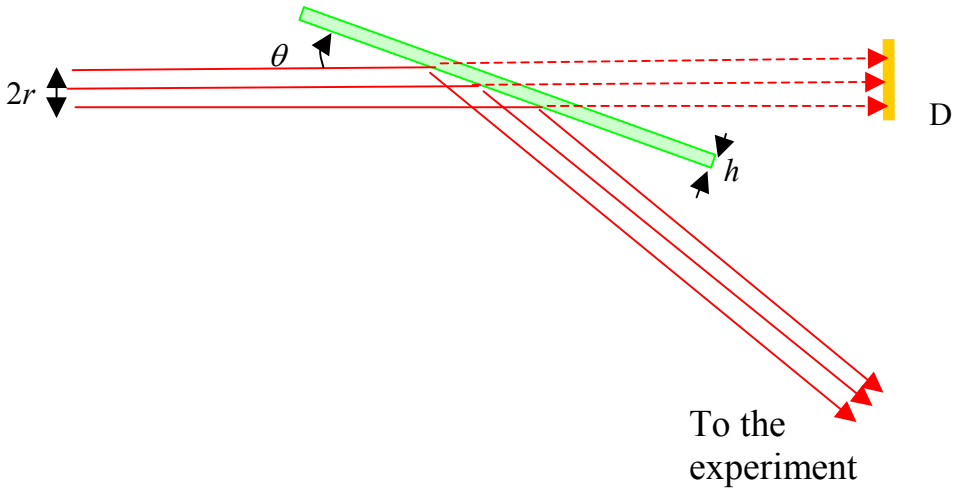

Fig. 8. Using a multilayer (shown as a green plate) to deflect an 800 eV beam. To remove the third harmonic (2.4 keV) in the detection system, one may need to use one more thin mirror in the diagnostic arm (dashed arrows).